Journal of Power Sources 224 (2013) 6–12

Contents lists available at SciVerse ScienceDirect

Journal of Power Sources

journal homepage: www.elsevier.com/locate/jpowsour

Carbon supported Pt–Sn nanoparticles as anode catalyst for direct borohydride–hydrogen peroxide fuel cell: Electrocatalysis and fuel cell performance

Lanhua Yi, Li Liu, Xingyan Wang, Xue Liu, Wei Yi, Xianyou Wang*

Key Laboratory of Environmentally Friendly Chemistry and Applications of Ministry of Education, School of Chemistry, Xiangtan University, Xiangtan 411105, Hunan Province, PR China

HIGHLIGHTS

- The Pt–Sn/C electrocatalysts were synthesized by a modified $NaBH_4$ reduction method.
- The average particle size of Pt–Sn nanoparticles is approximately 3 nm.
- The Sn-doping can apparently improve the electrocatalytic activity for the BH_4^- electrooxidation.
- The performance of DBHFC employing Pt–Sn/C as anode catalyst was reported.
- The maximum power density as high as 91.5 mW cm^{-2} was obtained at 25 °C.

ARTICLE INFO

Article history:
Received 5 July 2012
Received in revised form
18 September 2012
Accepted 20 September 2012
Available online 28 September 2012

Keywords:
Direct borohydride–hydrogen peroxide fuel cell
Anode electrocatalyst
Borohydride oxidation
Catalytic activity

ABSTRACT

Carbon supported Pt–Sn bimetallic nanoparticles (Pt–Sn/C) are prepared by a modified $NaBH_4$ reduction method in aqueous solution at room temperature, and used as the anode electrocatalyst for direct borohydride–hydrogen peroxide fuel cell (DBHFC). The physical and electrochemical properties of the as-prepared electrocatalysts are investigated by X-ray diffraction (XRD), transmission electron microscopy (TEM), cyclic voltammetry (CV), chronoamperometry (CA) and fuel cell test. XRD results show that the diffraction peaks in Pt–Sn/C catalyst shift slightly to lower 2θ values with the increase of Sn content compared with that of Pt/C catalyst, suggesting the formation of Pt–Sn alloying. TEM results show that the morphologies of Pt–Sn bimetallic nanoparticles are uniformly spherical with the particle size of about 3 nm on the carbon surface. Besides, it has been found that the Pt–Sn/C catalysts have much higher catalytic activity for the direct oxidation of BH_4^- than Pt/C catalyst, especially the $Pt_{67}Sn_{33}$/C catalyst presents the highest catalytic activity among all as-prepared catalysts. The DBHFC with $Pt_{67}Sn_{33}$/C anode catalyst and Pt/C cathode catalyst obtains the maximum power density as high as 91.5 mW cm^{-2} at 25 °C.

1. Introduction

In recent years, direct borohydride–hydrogen peroxide fuel cell (DBHFC), which is comprised of BH_4^- oxidation at the anode and H_2O_2 reduction at the cathode, have attracted considerable research interest due to their higher theoretical voltage, higher hydrogen storage density and faster anodic kinetics in comparison with hydrogen or methanol fuel cells [1–5]. In addition, DBHFCs do not suffer from CO poisoning which affects the catalytic activity of the catalysts and do not emit CO_2, the environmentally unfriendly gases, to the atmosphere. Furthermore, DBHFC is a liquid-feed type fuel cell, compared with the hydrogen proton exchange membrane fuel cells (PEMFCs), it also has the advantages of easier fuel delivery and storage, no cooling or humidification need and simpler design.

The anode reaction in an aqueous alkaline medium according to an eight-electron process is described as following [4,5]:

$$BH_4^- + 8OH^- \rightarrow BO_2^- + 6H_2O + 8e^- \quad E^0 = -1.24\ \text{V vs. SHE} \tag{1}$$

With the oxidation of $NaBH_4$ at the anode, the hydrogen peroxide in an acid electrolyte instead of oxygen as an oxidant can yield higher cell potential and energy density:

* Corresponding author. Tel.: +86 731 5829060; fax: +86 731 58292061.
E-mail address: wxianyou@yahoo.com (X. Wang).

0378-7753/$ – see front matter © 2012 Elsevier B.V. All rights reserved.
http://dx.doi.org/10.1016/j.jpowsour.2012.09.082

$$H_2O_2 + 2H^+ + 2e^- \rightarrow 2H_2O \quad E^0 = 1.77\ V\ vs.\ SHE \tag{2}$$

In combination with the reduction of hydrogen peroxide, DBHFC can give a theoretical cell voltage of 3.01 V and present a high energy density. Over cell reaction is as follow:

$$BH_4^- + 4H_2O_2 \rightarrow BO_2^- + 6H_2O \quad E^0_{cell} = 3.01\ V \tag{3}$$

The anode electrocatalyst is the key component in advancing the application of DBHFC. In the past few years, various materials have been studied as the anode electrocatalyst for the oxidation of BH_4^-, such as noble metals (Pt [1,2,6–8], Au [1,3–5,8–10], Os [11,12], Pd [13], Ag [14]), transition metals (Ni [15], Zn [16]) and hydrogen storage alloys [17].

To date, Pt is the most widely used catalyst material in fuel cells, but its high cost hinders a large-scale application in the fuel cell technologies. One promising way to lower the Pt catalyst costs is to alloy Pt with transition metals. Moreover, the Pt-based catalysts which alloyed with various transition metals have been claimed to be more active than pure Pt, and some of these catalysts have been reported to be two-fold more active [18–20]. Wang et al. [21] investigated Pt–Ni/C as anode electrocatalyst for the DBFC, and found that the addition of Ni to Pt/C results in the improvement of the electrocatalytic activity. Gyenge et al. [22] studied the DBFC using carbon supported Pt and Pt-alloys (Pt–Ir/C, Pt–Ni/C, and Pt–Au/C) as anode catalyst, and found that Pt–Ir/C and Pt–Ni/C gave the higher cell voltage at a given superficial current density than Pt/C and Pt–Au/C. Pt–Sn/C has been widely used as the electrocatalyst for methanol oxidation [23,24] and ethanol oxidation [25–34]. Tarozaitė et al. [35] prepared three forms Pt–Sn complexes of $H_3[Pt(SnCl_3)_5]$, $H_2[Pt(SnCl_3)_2Cl_2]$ and $H_2[Pt_3(SnCl_3)_8]$, and the BH_4^- electrooxidation on the glassy carbon (GC) electrode modified by the three complexes solution were studied respectively. However, to the best of our knowledge, carbon supported Pt–Sn bimetallic nanoparticles (Pt–Sn/C) as anodic catalyst for BH_4^- electrooxidation and the fuel cell performance of DBFC using Pt–Sn/C as anode catalyst were rarely studied.

In previous studies, we have studied the electrochemical properties of carbon supported Pt–Cu [36] and Pt–Co [37] bimetallic nanoparticles as anode electrocatalyst in DBHFC and found that the bimetallic catalysts showed much higher catalytic activity than monometallic Pt catalyst. In this work, a series of Pt–Sn/C catalysts were prepared by a modified $NaBH_4$ reduction method in aqueous solution at room temperature, and used as the anode catalyst for BH_4^- electrooxidation. The electrochemical evaluations of catalytic activity for the as-prepared catalysts were carried out by cyclic voltammetry and chronoamperometry. Moreover, the performances of the DBHFCs with Pt–Sn/C anode catalyst and Pt/C cathode catalyst were studied in detail.

2. Experimental methods

All chemical reagents were of analytical grade: sodium borohydride (AlfaAesar, 98%), hexachloroplatinicacid (Sigma–Aldrich), Stannous chloride dihydrate (Sigma–Aldrich), Polyvinylpyrrolidone (Sigma–Aldrich), Vulcan XC-72R carbon (Cabot Corp., 240 $m^2\ g^{-1}$) and Nafion solution (Dupont, 5 wt.%).

2.1. Preparation of Pt–Sn/C catalysts

$H_2PtCl_6 \cdot 6H_2O$ and $SnCl_2 \cdot 2H_2O$ were used as precursors of Pt–Sn/C catalysts. Vulcan XC-72R carbon black and $NaBH_4$ was used as support and reducing agent, respectively, Polyvinylpyrrolidone (PVP) was used to prevent nanoparticles from aggregating in the solution. Following is a brief description of the preparation method: the required amounts of H_2PtCl_6, $SnCl_2$, carbon and PVP were added to 300 ml deionized (DI) water under vigorous stirring for 30 min. Then, pH of the mixed solution was adjusted to 10 by adding 3 M NaOH solution, and 1 ml of 1 M $NaBH_4$ was added dropwise. After an additional 24 h of stirring, the resulting catalyst was filtered and washed with deionized water until no Cl^- was detected, then dried for 12 h at 80 °C in vacuum to obtain Pt–Sn/C catalysts. The atomic ratios of Pt/Sn which contained in the impregnation solutions were 100:0, 80:20, 75:25, 67:33 and 50:50, and the corresponding five catalysts were denoted as Pt/C, $Pt_{80}Sn_{20}$/C, $Pt_{75}Sn_{25}$/C, $Pt_{67}Sn_{33}$/C and $Pt_{50}Sn_{50}$/C, respectively. The loading of metals in all five materials is 20 wt.%.

2.2. Physical characterization of Pt–Sn/C electrocatalysts

The structure and morphology of Pt–Sn/C electrocatalysts were examined by TEM (JEM-3010, JEOL) operated at 300 kV. For TEM analyses, samples were prepared by adding one or two drops of the suspension, which was made by ultrasonically dispersing the catalyst in ethanol, onto the carbon-coated copper grid and drying it in air at room temperature.

X-ray diffractometer (D/MAX-3C) was employed with Cu Kα radiation ($\lambda = 1.54056$ Å) and a graphite monochromator at 50 kV, 100 mA to obtain X-ray diffraction (XRD) patterns of the samples. The 2θ angular regions between 20° and 90° were explored at a scan rate of 4° min^{-1}.

2.3. Electrochemical performance of anode catalysts

Electrochemical measurements were performed using CHI660A Electrochemistry Workstation and a typical three-electrode one-compartment electrolysis cell. The Pt–Sn/C or Pt/C was used as working electrode, a Ni foam mesh with 3 × 5 cm as counter electrode and an Ag/AgCl, KCl_{std} as the reference electrode. The electrolyte was 0.1 M $NaBH_4$ + 3.0 M NaOH. The working electrode was prepared as follows: 10 mg of Pt–Sn/C or Pt/C catalyst powder was dispersed by ultrasonic for 2 h in 1 ml blend solution of 0.25 ml 5 wt.% Nafion solution and 0.75 ml de-ionized water. Then 5 μl of slurry was pasted on the surface of the glassy carbon (GC) electrode (3 mm in diameter) which was polished to mirror by 0.5 μm alumina and sonicated 5 min prior to use. The dispersed catalyst on the GC surface was dried for 5 h at room temperature and the loading mass of catalyst was 0.7 mg cm^{-2} and actual metal loading mass on electrode is 0.14 mg cm^{-2}.

2.4. Fuel cell test

The catalysts ink was made by mixing isopropyl alcohol with 7 wt.% of Nafion solution and carbon supported catalysts. Then the ink were coated onto a stainless steel gauze resulting in a 4.5 mg cm^{-2} loading, and actual metal loading mass on electrode is 0.9 mg cm^{-2}. The catalyst electrodes were dried at 50 °C for 8 h in vacuum, then pressed at 10 MPa for 1 min to ensure a good electric contact.

The cell performance was tested against a Pt/C cathode and a Pt–Sn/C or Pt/C anode. A schematic diagram of the experimental set-up was shown in Fig. 1. A Nafion 117 membrane was used to separate the anolyte and catholyte. The anolyte is composed of 1 M $NaBH_4$ + 3 M NaOH, and the catholyte is composed of 2 M H_2O_2 + 0.5 M H_2SO_4. The fresh anolyte and catholyte were continuously supplied and withdrawn from the cell at 0.7 ml min^{-1}, respectively. The load was applied in steps of 5 mA within the range of 0–120 mA. Each step lasted 2 min and the current was continuously applied from one value to next without disconnecting the cell. The electrochemical testing of the cell was performed using

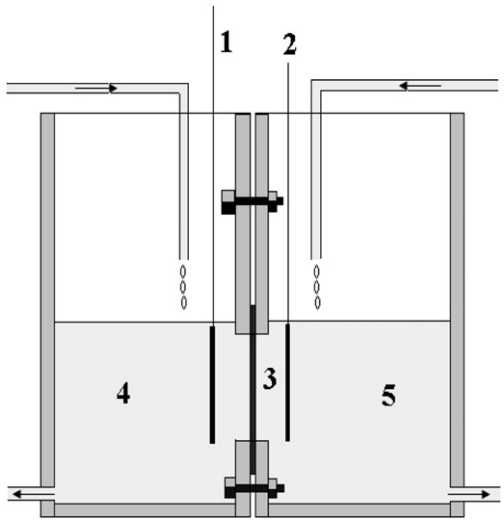

Fig. 1. Schematic illustration of DBHFC. (1) Anode catalyst, (2) cathode catalyst, (3) the activated Nafion 117 membrane, (4) 1 M $NaBH_4$ + 3.0 M NaOH, (5) 2 M H_2O_2 + 0.5 M H_2SO_4.

a battery testing system (BTS-51800, Neware Technology Co. Ltd., China). Power densities were calculated from the applied current and steady state potential.

3. Results and discussion

3.1. Physical characterization

Fig. 2 illustrates the XRD patterns of the Pt/C, $Pt_{80}Sn_{20}$/C, $Pt_{75}Sn_{25}$/C, $Pt_{67}Sn_{33}$/C and $Pt_{50}Sn_{50}$/C. The wide diffraction peak located at a 2θ value of about 25° is attributed to carbon (002) crystal face, which matches well with the standard C peak (JCPDS No. 75-1621). The diffraction peaks positioned at 2θ = 39°, 46°, 67° and 81° could be indexed to the (111), (200), (220) and (311) planes of face-centered cubic (fcc) Pt, which match well with the standard Pt peaks (JCPDS No. 04-0802). There are no diffraction peaks for Sn or its oxides in the XRD patterns of Pt–Sn/C, but their presence cannot be discarded because they may be existed in an amorphous

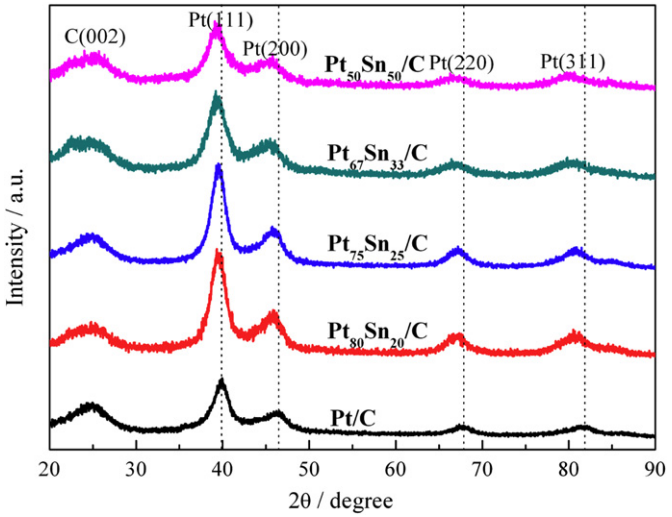

Fig. 2. XRD patterns of Pt/C and Pt–Sn/C with different Pt/Sn atomic ratios.

form [38]. The diffraction peaks are shifted to lower 2θ values for the Pt–Sn/C catalysts compared with the corresponding peaks in the Pt/C catalyst, and the extent of 2θ value shift will increase with the increase of Sn content.

The diffraction peak for Pt (220) is used to estimate the particle size by the Scherrer's equation [23]:

$$D = \frac{0.9\lambda}{B\cos\theta} \tag{4}$$

where D is average particle size, nm, λ is the X-ray wavelength (1.54056 Å for Cu Kα radiation), B is the full width at half-maximum in radians (FWHM) and θ is the angle of Pt (220) peak. The calculated average particle size of Pt, $Pt_{80}Sn_{20}$, $Pt_{75}Sn_{25}$, $Pt_{67}Sn_{33}$, and $Pt_{50}Sn_{50}$ nanoparticles dispersed on carbon are 3.6 nm, 3.2 nm, 3.2 nm, 2.8 nm, 2.8 nm, respectively.

The lattice parameter (a_{fcc}) values for the Pt–Sn/C and Pt/C catalysts are calculated by using Pt (220) peak according to Bragg formula [23]:

$$a_{fcc} = \frac{\sqrt{2}\lambda}{\sin\theta} \tag{5}$$

The calculated lattice parameter of Pt/C, $Pt_{80}Sn_{20}$/C, $Pt_{75}Sn_{25}$/C, $Pt_{67}Sn_{33}$/C and $Pt_{50}Sn_{50}$/C catalysts are 0.3918 nm, 0.3945 nm, 0.3949 nm, 0.3961 nm, 0.3973 nm, respectively. The lattice parameter of Pt/C catalyst (a = 0.3918 nm) is smaller than that of the bulky Pt metal (JCPDS No. 04-0802, a = 0.3923 nm), which has been ascribed to the interactions or size effect between Pt and carbon [29,39]. The addition of Sn will lead to enlargement of the lattice parameter of the catalysts. So, the lattice parameters of all Pt–Sn/C catalysts are larger than that of Pt/C. It is probably because the atomic size of Sn (R_{Sn} = 1.61 Å) is bigger than that of Pt (R_{Pt} = 1.39 Å), and the addition of some amount of Sn to Pt/C induce the extension of Pt crystal structure. From literature data [29,31], a linear relationship of the lattice parameter and alloyed Sn atomic ration has been proposed by the following equation [29,31]:

$$x_{Sn} = \frac{a_{PtSn} - a_{Pt}}{k} \tag{6}$$

where x_{Sn} describes the atomic ration in the alloy, a_{Pt} = 0.3918 nm is the lattice parameter of Pt/C and k is a constant, 0.0352 nm [31]. Based on Vegard's law, the alloying degree, Sn_{alloy}, in the bimetallic catalysts is determined by the follow equation [29,31,32]:

$$Sn_{alloy} = \frac{x_{Sn}}{(1 - x_{Sn})(Sn/Pt)_{nom}} \tag{7}$$

here x_{Sn} is calculated from Eq. (6), $(Sn/Pt)_{nom}$ is the nominal Sn/Pt atomic ratio. The calculated results of the Sn alloying degree in the $Pt_{80}Sn_{20}$/C, $Pt_{75}Sn_{25}$/C, $Pt_{67}Sn_{33}$/C and $Pt_{50}Sn_{50}$/C are about 33.2%, 29.3%, 27.8% and 18.5%, respectively. The results show that the alloying degree decreases with the increase of Sn content, and the amount of Sn alloyed with Pt is smaller than their nominal content. It is further confirmed that the existence of Sn which is present as amorphous species, most likely oxides, on the Pt–Sn/C catalysts, although it cannot be detected by XRD.

The morphology and distribution of the catalysts were observed by TEM. Because the preparation methods of Pt–Sn/C catalysts were identical, the morphology and structure of as-prepared Pt–Sn/C catalysts were similar. In present, the $Pt_{67}Sn_{33}$/C catalyst was chosen as the representative to analysis. Fig. 3a is the TEM image of the Pt/C catalyst, and Fig. 3b and c are the TEM and HR-TEM images of $Pt_{67}Sn_{33}$/C catalysts respectively. Fig. 3 indicates that the metal nanoparticles are uniformly dispersed on the surface of carbon with

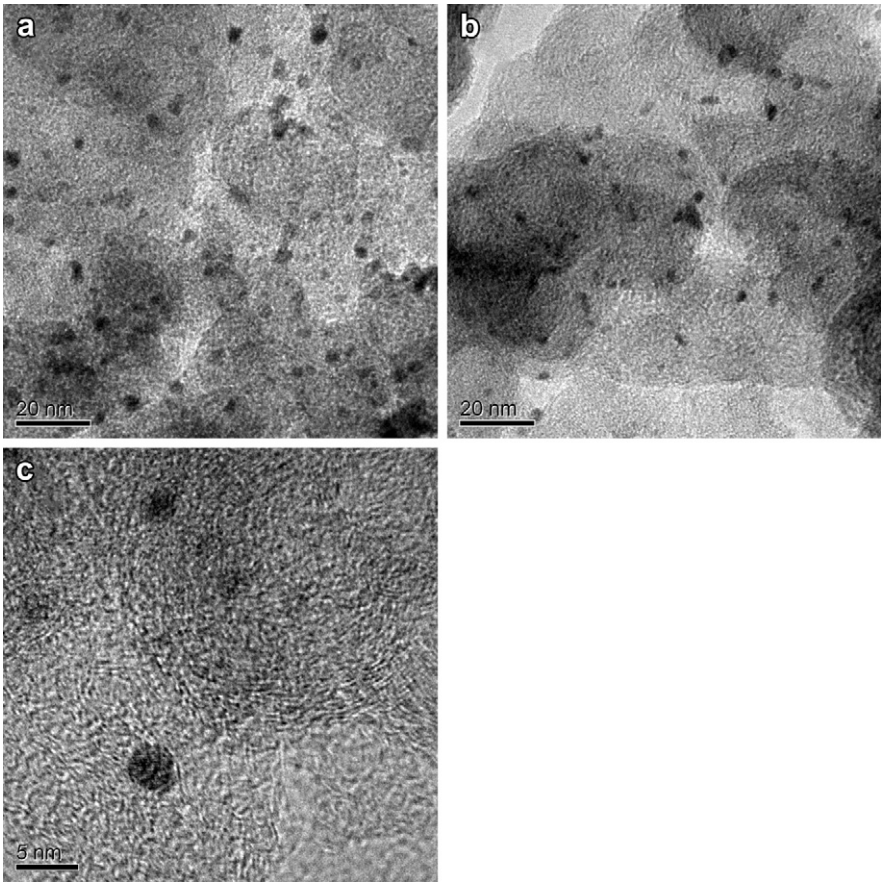

Fig. 3. TEM images of (a) Pt/C and (b, c) $Pt_{67}Sn_{33}$/C.

a narrow particle size distribution. The morphology of the metal nanoparticles is generally spherical, and the mean diameter is approximately 3.5 nm and 3 nm for Pt/C and $Pt_{67}Sn_{33}$/C catalysts, respectively, which is well consistent with the XRD results.

3.2. Electrochemical characterization

3.2.1. Cyclic voltammetry

The cyclic voltammetries recorded for Pt/C, $Pt_{80}Sn_{20}$/C, $Pt_{75}Sn_{25}$/C, $Pt_{67}Sn_{33}$/C and $Pt_{50}Sn_{50}$/C electrodes with 0.1 M $NaBH_4$ + 3.0 M NaOH solution at a scan rate of 20 mV s^{-1} in the potential range of −1.2 V to 0.6 V (vs. Ag/AgCl, KCl_{std}) are showed in Fig. 4. The Pt–Sn/C and Pt/C electrodes show a similar catalytic behavior for the electrooxidation of BH_4^- by comparing the shapes of all CV curves between −1.2 and 0.6 V vs. Ag/AgCl, KCl_{std}. According to the CV curves, the electrochemical behavior of BH_4^- is fairly complex characterized by a number of oxidation peaks. During the forward sweep, at a rate of 20 mV s^{-1}, a well-defined oxidation peak occurs at about −0.8 V (a1), followed by a broad hump anodic peak (a2) is observed. During the reverse sweep, a sharp anodic spike (c1) is observed. Similar anodic-cathodic peak patterns in cyclic voltammetry have reported by Concha and Chatenet [7] and Gyenge [8]. The first anodic peak (a1) can be assigned to borohydride hydrolysis followed by the electro-oxidation of H_2, the second oxidation peak (a2) is attributed to the direct oxidation of BH_4^- in absence of H_2 electrooxidation, and the peak (c1) is due to the oxidation of absorbed intermediate oxidation products of BH_3OH^- (Eq. (9)) on the partially oxidized Pt surface [7,8].

$$BH_4^- + H_2O \rightarrow BH_3OH^- + H_2 \quad (8)$$

$$BH_3OH^- + 3OH^- \rightarrow BO_2^- + \frac{3}{2}H_2 + 2H_2O + 3e^- \quad (9)$$

For direct oxidation of BH_4^-, the anodic current densities of peak a2 on Pt/C, $Pt_{80}Sn_{20}$/C, $Pt_{75}Sn_{25}$/C, $Pt_{67}Sn_{33}$/C and $Pt_{50}Sn_{50}$/C are

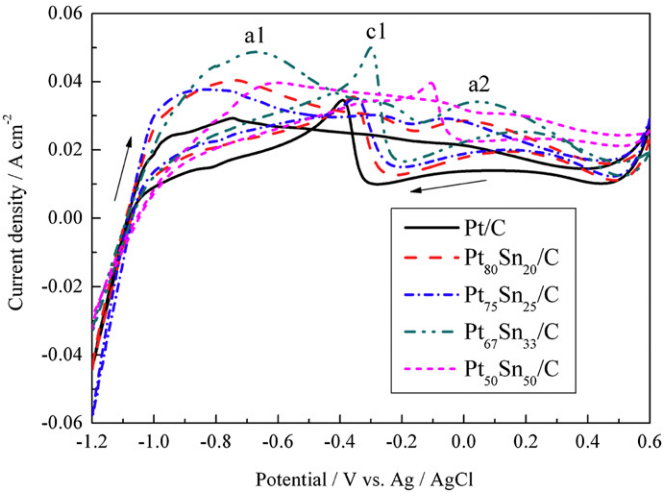

Fig. 4. Cyclic voltammograms of Pt/C and Pt–Sn/C electrodes in 0.1 M $NaBH_4$ + 3.0 M NaOH at a potential scan rate of 20 mV s^{-1}.

21.88 mA cm^{-2}, 28.51 mA cm^{-2}, 29.19 mA cm^{-2}, 34.10 mA cm^{-2}, and 30.60 mA cm^{-2}, respectively. Although the content of Pt in Pt–Sn/C catalysts is less than that in Pt/C catalyst, the peak current densities on Pt–Sn/C electrodes do not reduce. On the contrary, all the peak current densities for a2 on Pt–Sn/C electrodes are much higher than that on Pt/C electrode. Compared with Pt/C electrocatalyst, the current densities of peak a2 on $Pt_{80}Sn_{20}$/C, $Pt_{75}Sn_{25}$/C, $Pt_{67}Sn_{33}$/C and $Pt_{50}Sn_{50}$/C electrodes are increased 30.30%, 33.41%, 55.85% and 39.85%, respectively, indicating that the Pt–Sn/C electrocatalysts can obviously improve the catalytic activity for BH_4^- oxidation. It can be attributed to the synergistic effect of Pt–Sn bimetallic nanoparticles, which jointly improves the electrochemical oxidation of BH_4^- [5]. Among the five electrodes, the peak current density of a2 on the $Pt_{67}Sn_{33}$/C electrode is the highest, thus the $Pt_{67}Sn_{33}$/C catalyst will show the highest catalytic activity for the electrooxidation of BH_4^-. In addition, Pt–Sn/C also reduces the cost of electrocatalyst, and it will be a promising anode electrocatalyst for the application of DBHFC.

3.2.2. Chronoamperometry

Chronoamperometric technique is another effective method to evaluate the electrocatalytic activity of catalysts. Fig. 5a shows the chronoamperometric responses of the Pt/C, $Pt_{80}Sn_{20}$/C, $Pt_{75}Sn_{25}$/C, $Pt_{67}Sn_{33}$/C and $Pt_{50}Sn_{50}$/C electrodes in 0.1 M $NaBH_4$ + 3.0 M NaOH solution from −1.2 to −0.2 V vs. Ag/AgCl, KCl_{std}. It can be found from Fig. 5a that all five samples show current decay during the electrooxidation process of BH_4^-. After the application of the set potential for 60 s, the Pt–Sn/C electrodes deliver higher current density than the Pt/C electrode. The current densities for the Pt/C, $Pt_{80}Sn_{20}$/C, $Pt_{75}Sn_{25}$/C, $Pt_{67}Sn_{33}$/C and $Pt_{50}Sn_{50}$/C are 18.83 mA cm^{-2}, 23.99 mA cm^{-2}, 30.91 mA cm^{-2}, 39.08 mA cm^{-2}, and 32.46 mA cm^{-2}, respectively. Apparently, the sequence of catalytic activity of five electrodes is $Pt_{67}Sn_{33}$/C > $Pt_{50}Sn_{50}$/C > $Pt_{75}Sn_{25}$/C > $Pt_{80}Sn_{20}$/C > Pt/C. It is further demonstrated that $Pt_{67}Sn_{33}$/C catalyst exhibits the best catalytic performance among the all five electrodes. Such results further demonstrated that the addition of Sn can greatly improve the catalytic activity of Pt catalyst for the BH_4^- electrooxidation.

The Cottrell plot obtained from the chronoamperometry results was presented in Fig. 5b. As show in Fig. 5b, $it^{1/2}$ increases with time on each catalyst electrodes, indicating that the processes of BH_4^- electrooxidation on Pt/C and Pt–Sn/C electrodes are not controlled by the diffusion of BH_4^-, and BH_4^- is consumed at the outer edge of the catalyst layer, that is, at the bulk electrolyte solution-catalyst layer interface. It also indicates that under the employed experimental conditions, neither the intra-catalyst layer diffusion nor the

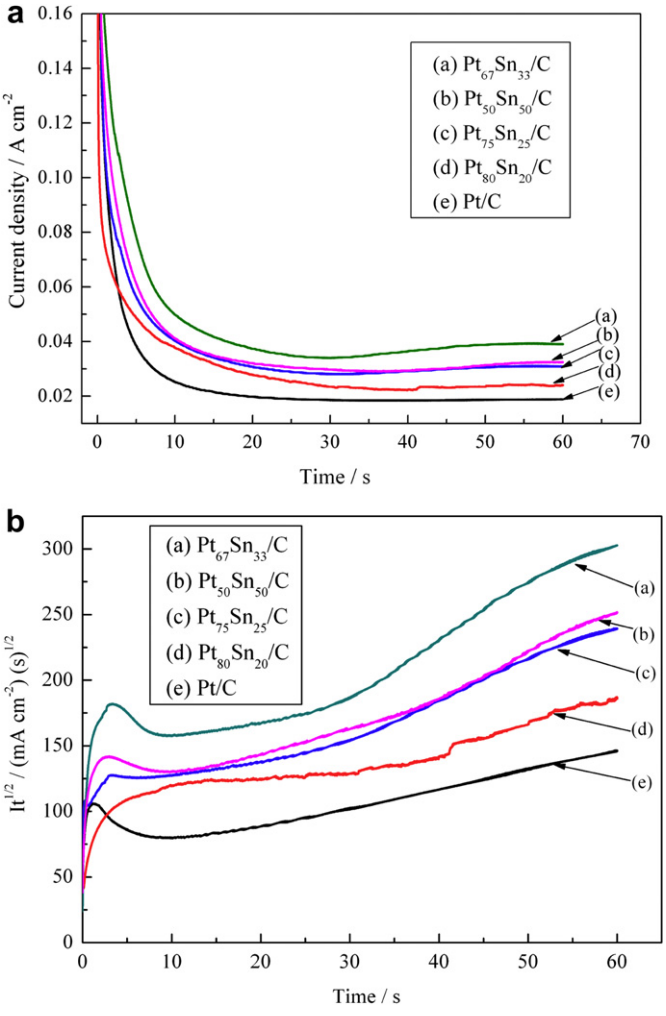

Fig. 5. (a) Chronoamperometry curves of Pt/C and Pt–Sn/C electrodes in 0.1 M $NaBH_4$ + 3 M NaOH at 25 °C and (b) Cottrell plot generated from the chronoamperometry data. Potential step from −1.2 to −0.2 V vs. Ag/AgCl, KCl_{std}.

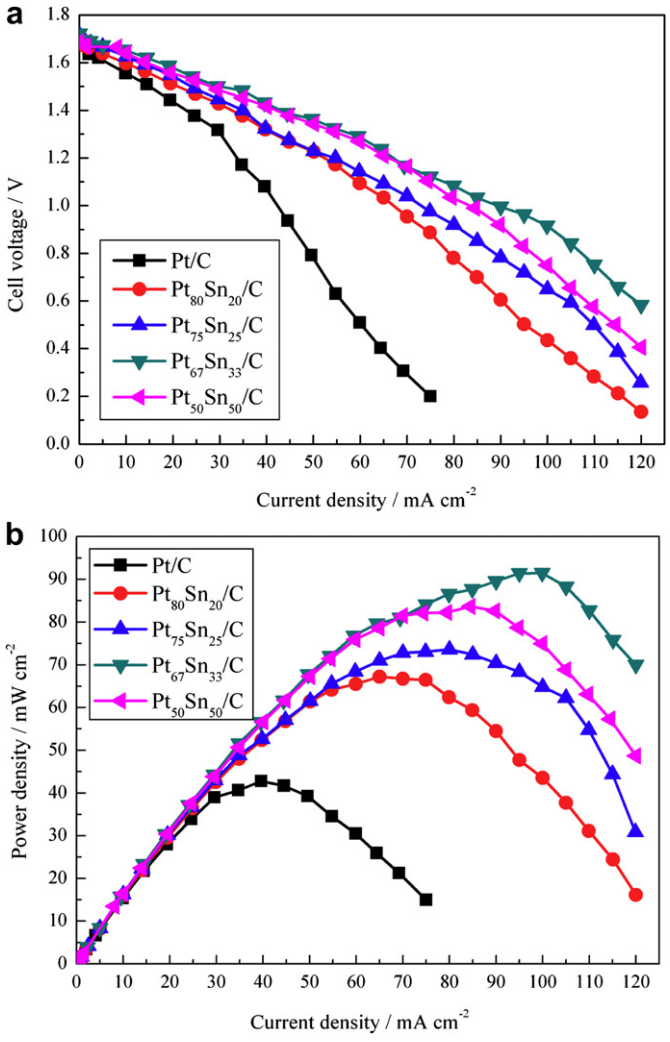

Fig. 6. (a) Cell polarization curves and (b) power density curves of the DBHFCs using Pt/C and Pt–Sn/C anode catalysts at 25 °C with 1 M $NaBH_4$ + 3 M NaOH anolyte and 2 M H_2O_2 + 0.5 M H_2SO_4 catholyte.

Table 1
The comparison of DBFC performances using different anode catalysts.

Anode catalyst	Cathode catalyst	Membrane	Fuel	Oxidation	Power density (mW cm^{-2})	T (°C)	Mass activity basis (W g^{-1} anode catalyst)	Ref.
$Au_{45}Co_{55}$/C (0.9 mg metal cm^{-2})	Au/C (0.9 mg Pt cm^{-2})	Nafion 117	1 M $NaBH_4$ + 3 M NaOH	2 M H_2O_2 + 0.5 M H_2SO_4	66.5	25	73.9	[4]
$Au_{58}Ni_{42}$/C (0.9 mg metal cm^{-2})	Au/C (0.9 mg Pt cm^{-2})	Nafion 117	1 M $NaBH_4$ + 3 M NaOH	2 M H_2O_2 + 0.5 M H_2SO_4	45.7	20	50.8	[5]
Au/C (0.5 mg Au cm^{-2})	Pt/C (4 mg Pt cm^{-2})	Nafion 117	25% $NaBH_4$ + 6 M NaOH	1 M H_2O_2 + 1 M HCl + 3 M NaCl	34	20	68	[1]
Os/C (1 mg Os cm^{-2})	Pt black (4 mg Pt cm^{-2})	Nafion 117	0.5 M $NaBH_4$ + 2 M NaOH	O_2 Flowrate: 1.25 l min^{-1}	18	25	18	[11]
					69	60	69	
Pt–Ni/C(mole, 1:1) (5 mg metal cm^{-2})	Pt/C (4 mg Pt cm^{-2})	Nafion 117	2 M $NaBH_4$ + 2 M NaOH	O_2 Flowrate: 0.2 l min^{-1}	53	60	10.6	[22]
$Pt_{50}Cu_{50}$/C (0.9 mg metal cm^{-2})	Pt/C (0.9 mg Pt cm^{-2})	Nafion 117	1 M $NaBH_4$ + 3 M NaOH	2 M H_2O_2 + 0.5 M H_2SO_4	71.6	25	79.6	[36]
$Pt_{67}Co_{33}$/C (0.9 mg metal cm^{-2})	Pt/C (0.9 mg Pt cm^{-2})	Nafion 117	1 M $NaBH_4$ + 3 M NaOH	2 M H_2O_2 + 0.5 M H_2SO_4	79.7	25	88.6	[37]
Pt/C (0.9 mg Pt cm^{-2})	Pt/C (0.9 mg Pt cm^{-2})	Nafion 117	1 M $NaBH_4$ + 3 M NaOH	2 M H_2O_2 + 0.5 M H_2SO_4	42.8	25	47.6	
$Pt_{67}Sn_{33}$/C (0.9 mg metal cm^{-2})	Pt/C (0.9 mg Pt cm^{-2})	Nafion 117	1 M $NaBH_4$ + 3 M NaOH	2 M H_2O_2 + 0.5 M H_2SO_4	91.5	25	101.7	

external mass transfer of BH_4^- limit the BH_4^- electrooxidation rate [40]. Furthermore, the increase of the $it^{1/2}$ function is also an indication that the electrode surface is not poisoned during the time course of the experiment. Moreover, the highest value of $it^{1/2}$ for $Pt_{67}Sn_{33}$/C electrode among all five electrodes further demonstrates the $Pt_{67}Sn_{33}$/C catalyst has the highest electrocatalytic activity for the BH_4^- electrooxidation, and it is also expected that the DBHFC with $Pt_{67}Sn_{33}$/C anode catalyst will exhibit the highest power output.

3.3. Single fuel cell performance

Fig. 6 shows the changes of cell voltage and power density of DBHFCs with current density at 25 °C using Pt/C, $Pt_{80}Sn_{20}$/C, $Pt_{75}Sn_{25}$/C, $Pt_{67}Sn_{33}$/C and $Pt_{50}Sn_{50}$/C as anode catalysts. The cathode catalysts of all DBHFCs systems were Pt/C. The anolyte was 1 M $NaBH_4$ + 3 M NaOH solution, and the catholyte was 2 M H_2O_2 + 0.5 M H_2SO_4 solution according to our previous studies [4,5,36,37]. The open circuit voltage (OCV) of the cell is about 1.7 V, which is lower than the standard cell potential for the DBHFC with acid catholyte. The low value is probably caused by mixed potential at the anode and cathode from simultaneous oxidation of BH_4^- ions and hydrogen at the anode and reduction of H_2O_2 and O_2 at the cathode [41]. As shown in Fig. 6a, the cell voltage presents nearly a linear decrease with the increase of current density due to much higher polarization at higher density. However, the DBHFCs with Pt–Sn/C anode have smaller polarization for BH_4^- oxidation than the one with Pt/C anode for the reason of Pt–Sn alloy can improve the performance of DBHFC. The maximum power densities of the DBHFCs using Pt/C, $Pt_{80}Sn_{20}$/C, $Pt_{75}Sn_{25}$/C, $Pt_{67}Sn_{33}$/C and $Pt_{50}Sn_{50}$/C as anode at 25 °C are 42.8 mW cm^{-2}, 67.2 mW cm^{-2}, 73.6 mW cm^{-2}, 91.5 mW cm^{-2} and 83.7 mW cm^{-2}, respectively, and the DBHFC using $Pt_{67}Sn_{33}$/C as anode catalyst exhibits the best performance (Fig. 6b). For comparison, the DBFCs performances using different anode electrocatalysts is tabulated in Table 1. Apparently, the $Pt_{67}Sn_{33}$/C anode catalyst shows very excellent performance among these catalysts listed in Table 1. Therefore, $Pt_{67}Sn_{33}$/C could be a promising catalyst to make less expensive DBHFC.

4. Conclusions

In the present study, Pt–Sn/C electrocatalyst was facilely prepared by a modified $NaBH_4$ reduction method in aqueous solution at room temperature and used as anode electrocatalyst for DBHFCs. The Pt–Sn nanoparticles were uniformly dispersed on the carbon support with average particle size approximately 3 nm. The Pt–Sn/C catalysts represent much higher electrochemical catalytic activity for BH_4^- electrooxidation than Pt/C catalyst in the alkaline solution for the reason that Sn-doping can significantly improve the electrocatalytic activity of the catalyst. Among the as-prepared five catalysts, $Pt_{67}Sn_{33}$/C reveals the highest electrocatalytic activity to the direct oxidation of BH_4^-, and the DBHFC employing $Pt_{67}Sn_{33}$/C as anode catalyst and Pt/C as cathode catalyst obtained the maximum power density as high as 91.5 mW cm^{-2} at 25 °C. Therefore, the Pt–Sn/C catalysts with high performance and low cost can be used as a promising anode catalyst for DBFCs.

Acknowledgments

This work was financially supported by the National Natural Science Foundation of China (Grant Nos. 51272221, 51072173 and 21203161), Doctoral Fund of Ministry of Education of China (Grant No. 20094301110005) and the Scientific Research Fund of Hunan Provincial Education Department (Grant No. 11A118).

References

[1] C. Ponce de León, F.C. Walsh, A. Rose, J.B. Lakeman, D.J. Browning, R.W. Reeve, J. Power Sources 164 (2007) 441–448.
[2] R.K. Raman, S.K. Prashant, A.K. Shukla, J. Power Sources 162 (2006) 1073–1076.
[3] H. Cheng, K. Scott, J. Power Sources 160 (2006) 407–412.
[4] F. Pei, Y. Wang, X. Wang, P. He, Q. Chen, X. Wang, H. Wang, L. Yi, J. Guo, Int. J. Hydrogen Energy 35 (2010) 8136–8142.
[5] P.Y. He, Y. Wang, X.Y. Wang, F. Pei, H. Wang, L. Liu, L.H. Yi, J. Power Sources 196 (2011) 1042–1047.
[6] J.H. Kim, H.S. Kim, Y.M. Kang, M.S. Song, S. Rajendran, S.C. Han, J. Electrochem. Soc. 151 (2004) A1039–A1043.
[7] B.M. Concha, M. Chatenet, Electrochem. Acta 54 (2009) 6119–6129.
[8] E.L. Gyenge, Electrochem. Acta 49 (2004) 965–978.
[9] L.C. Nagle, J.F. Rohan, Int. J. Hydrogen Energy 36 (2011) 10319–10326.
[10] M.V. Mirkin, H. Yang, A.J. Bard, J. Electrochem. Soc. 139 (1992) 2212–2217.
[11] W.S.L. Vincent, E.L. Gyenge, J. Electrochem. Soc. 155 (2008) B1155–B1160.
[12] M.H. Atwa, D.O. Northwood, E.L. Gyenge, Int. J. Hydrogen Energy 30 (2005) 1323–1331.
[13] J.Q. Yang, B.H. Liu, S. Wu, J. Power Sources 194 (2009) 824–829.
[14] E. Sanli, H. Celikkan, B.Z. Uysal, M.L. Aksu, Int. J. Hydrogen Energy 31 (2006) 1920–1924.
[15] J. Ma, Y. Sahai, R.G. Buchheit, J. Power Sources 195 (2010) 4709–4713.
[16] D.M.F. Santos, C.A.C. Sequeira, J. Electrochem. Soc. 157 (2010) B13–B19.
[17] G.L. Wang, X.Y. Wang, R.R. Miao, D.X. Cao, K.N. Sun, Int. J. Hydrogen Energy 35 (2010) 1227–1231.
[18] D.A. Landsman, F.J. Luczak, U. S. Patent, 4,316,944 (1982).

[19] F.J. Luczak, D.A. Landsman, U. S. Patent, 4,447,506 (1984).
[20] F.J. Luczak, D.A. Landsman, U. S. Patent, 4,667,092 (1984).
[21] G.J. Wang, Y.Z. Gao, Z.B. Wang, C.Y. Du, J.J. Wang, G.P. Yin, J. Power Sources 195 (2010) 185–189.
[22] E. Gyenge, M. Atwan, D. Northwood, J. Electrochem. Soc. 153 (2006) A150–A158.
[23] D.H. Lim, D.H. Choi, W.D. Lee, H.I. Lee, Appl. Catal. B 89 (2009) 484–493.
[24] I. Honma, T. Toda, J. Electrochem. Soc. 150 (2003) A1689–A1692.
[25] L. Jiang, A. Hsu, D. Chu, R. Chen, Int. J. Hydrogen Energy 35 (2010) 365–372.
[26] K. Miecznikowski, P.J. Kulesza, J. Power Sources 196 (2011) 2595–2601.
[27] T.S. Almeida, K.B. Kokoh, A.R. De Andrade, Int. J. Hydrogen Energy 36 (2011) 3803–3810.
[28] L. Jiang, G. Sun, Z. Zhou, W. Zhou, Q. Xin, Catal. Today 93–95 (2004) 665–670.
[29] H. Li, G. Sun, L. Cao, L. Jiang, Q. Xin, Electrochim. Acta 52 (2007) 6622–6629.
[30] Y. Guo, Y. Zheng, M. Huang, Electrochim. Acta 53 (2008) 3102–3108.
[31] M. Zhu, G. Sun, Q. Xin, Electrochim. Acta 54 (2009) 1511–1518.
[32] L. Colmenares, H. Wang, Z. Jusys, L. Jiang, S. Yan, G.Q. Sun, R.J. Behm, Electrochim. Acta 52 (2006) 221–233.
[33] J.C.M. Silva, L.S. Parreira, R.F.B. De Souza, M.L. Calegaro, E.V. Spinacé, A.O. Neto, M.C. Santos, Appl. Catal. B 110 (2011) 141–147.
[34] A. Jablonski, A. Lewera, Appl. Catal. B 115–116 (2012) 25–30.
[35] R. Tarozaitė, L.T. Tamašiūnaitė, V. Jasulaitienė, J. Solid State Electrochem. 13 (2009) 721–731.
[36] L.H. Yi, B.A. Hu, Y.F. Song, X.Y. Wang, G.S. Zou, W. Yi, J. Power Sources 196 (2011) 9924–9930.
[37] L.H. Yi, Li Liu, Xue Liu, Xingyan Wang, Wei Yi, Peiying He, Xianyou Wang, Int. J. Hydrogen Energy 37 (2012) 12650–12658.
[38] D. Wang, S. Lu, S. Jiang, Electrochim. Acta 55 (2010) 2964–2971.
[39] A.K. Shukla, M.K. Ravikumar, A. Roy, S.R. Baraman, D.D. Sarma, A.S. Arico, V. Antonucci, L. Pino, N. Giordano, J. Electrochem. Soc. 141 (1994) 1517–1522.
[40] M.H. Atwan, C.L.B. Macdonald, D.O. Northwood, E.L. Gyenge, J. Power Sources 158 (2006) 36–44.
[41] C. Ponce de león, F.C. Walsh, C.J. Patrissi, M.G. Medeiros, P.R. Bessette, R.W. Reeve, J.B. Lakeman, A. Rose, D. Browening, Electrochem. Commun. 10 (2008) 1610–1613.